Silver-ion disorder in α-AgI: A computer simulation study

K. O'Sullivan
Department of Theoretical Physics, Oxford University, Keble Road, Oxford OX1 3NP, United Kingdom

G. Chiarotti
Laboratorio Avanzate Superfici e Catalisi (TASC), del Consorzio Interuniversitario di Fisica della Materia (INFM), Padriciano 99, I-34012 Trieste, Italy
and Scuola Internazionale Superiore di Studi Avanzati, Strada Costiera 11, I-34014 Trieste, Italy

P. A. Madden
Department of Physical Chemistry, Oxford University, South Parks Road, Oxford OX1 3QZ, United Kingdom
(Received 14 August 1990; revised manuscript received 26 December 1990)

Computer simulation studies of the superionic conducting α phase of AgI are described, which focus on the degree of disorder of the silver ions and the interpretation of experiments that reflect this property. Calculations of the diffuse x-ray scattering and of the Raman spectrum are compared with experimental data. The predictions of two theoretical schemes, which have sought to describe possible ordering phenomena of the silver ions, are critically examined.

I. INTRODUCTION

The ion-conducting α phase of AgI has been extensively studied experimentally,[1-5] theoretically,[6-9] and by computer simulation.[10-13] In this work we shall extend previous computer simulation analyses and examine various experimental results and theoretical predictions that bear upon the nature of the disorder of the silver in this phase. We shall make use of a potential model due to Rahman, Vashishta, and Parrinello (RVP),[10] which has successfully reproduced many properties of this material.[11,12]

The α phase is the stable phase of AgI between 420 and 830 K at normal pressure. The structure of the system can be understood as a bcc lattice of iodine ions with the silver cations occupying interstitial tetrahedral (Td) sites.[1,10] There are six such sites for each I^- and the Td sites can be regarded as forming six interpenetrating bcc sublattices. The Ag^+ ions are disordered over these sublattices. The ionic conduction mechanism involves the transport of silver ions in the stationary bcc iodine sublattice. The silver mobility is high, the diffusion coefficient has a value comparable to that of a normal liquid. Computer simulations with RVP potentials indicate[12] that the silver-ion motion involves migration between adjacent Td sites along the [110] direction of the crystal. These results are in good quantitative agreement with inelastic neutron-scattering data.[4] The calculated mobility is in very good agreement with experiment.[14]

At low temperature and normal pressure, AgI undergoes a transition to a β phase which does not show ionic conduction. This phase has a wurtzite crystal structure, which can be viewed as an ordered crystal consisting of a hexagonal lattice of iodines with the silvers occupying interstitial sites of the tetrahedral symmetry. In contrast to the α phase, only a single sublattice of Td sites is occupied in this crystal. A constant-stress molecular-dynamics simulation using the RVP potential gave the $\alpha \rightarrow \beta$ transition close to the correct temperature.[10] More recently, Tallonl[11] has conducted an extensive survey of the phase diagram predicted by the RVP potential. He has shown that it reproduces all the known phases of AgI with phase boundaries very close to the experimental ones.

A more detailed examination of the Ag^+ structure in the α phase is of interest because several observations suggest that a considerable degree of order exists. At the macroscopic level, it has been argued from the entropy change[15] associated with the $\alpha \rightarrow \beta$ transition that the Ag^+ ions are not randomly disposed on Td sites. Some heat-capacity[16] data has suggested the existence of a weak first-order transition within the α phase at a temperature of about 700 K associated with a change in the degree of silver order. Raman-scattering measurements show strong temperature-dependent changes in intensity and depolarization ratio[17,18] in the same temperature range and these have been interpreted as due to changes in the local order of the silver ions around the iodines, within a specific model. Changes in the silver order should influence the diffuse x-ray-scattering patterns which have been extensively studied by Cava and coworkers.[1]

Given the success of the RVP potential in reproducing the phase diagram, the mobility and the neutron-scattering data, it seems of interest to compare the Ag^+ ion structures predicted by this potential model with the experimental quantities which bear upon the Ag^+ ion disorder. Tallon[11] has already shown that the thermodynamic quantities calculated in the α phase at zero pressure are consistent with the existence of an order-disorder transition at a temperature close to the experimentally observed Raman and heat-capacity anomalies.

A further motive for studying the silver-ion order is to understand its relationship (if any) to the structural phase

transitions of the iodine lattice. It seems plausible to suggest that the reorganization of the iodine lattice from bcc to hexagonal at the $\alpha \rightarrow \beta$ transition occurs because the former becomes unstable as the silver ions become progressively more ordered on the interstitital sublattices. Again, we know from the RVP (Ref. 10) and Tallon[11] work that the potential is capable of reproducing this transition.

Several theoretical models have been proposed to describe effects of the partial ordering of the Ag^+ ions. The most sophisticated of these is due to Szabó, who treated the interactions of the Ag^+ ions on the Td sites with a lattice-gas model with the topology of six interpenetrating bcc sublattices and nearest-neighbor and next-nearest-neighbor interactions. Within a mean-field analysis, he showed that a rich variety of transitions between more or less ordered phases could occur in the model system, and suggested that the heat-capacity and Raman anomalies could be interpreted in these terms.

Our objective in this work is to analyze the silver disorder predicted by the RVP potential, to correlate this information with what is observed experimentally, and to critically examine the predictions of the theoretical models in the light of the simulation results.

II. SIMULATION METHODS

We have performed molecular-dynamics simulations using the standard constant volume, constant density, constant-energy (NVE) ensemble, with cubic periodic boundary conditions. We make use of the Beeman algorithm.[19] The potential used (RVP) is based on the idea discussed by Rahman and Vashishta in Ref. 10(a), with the parameters used in the succeeding paper by Rahman, Vashishta, and Parrinello.[10(b)] An Ewald summation is used to treat the Coulombic interactions.[19] Runs have been performed on systems containing 500, 864, and 1372 ions at various temperatures. In the data presented here, the lattice parameters have been kept fixed at a value of 5.256 Å, a value originally obtained from the experimental density close to the $\alpha \rightarrow \beta$ transition and used in Ref. 12. This corresponds to a molar volume of 43.6 cm^3. Other runs were done at molar volumes as high as 48 cm^3 with little effect on the results. Because of the constant density and the cubic simulation cell, both melting and the $\alpha \rightarrow \beta$ phase transition will be suppressed in our calculations. A time step of 0.4997×10^{-14} sec was used in all runs. Systems were equilibrated for 5000 steps (with a run at one temperature starting from the final configuration of another) and statistics gathered for 15 000 steps.

III. COMPARISON WITH X-RAY-SCATTERING EXPERIMENTS

The total intensity of x-ray scattering by the crystal is given by

$$S^{\text{tot}}(\mathbf{Q}) = S_{\text{AgAg}}(\mathbf{Q}) + 2S_{\text{AgI}}(\mathbf{Q}) + S_{\text{II}}(\mathbf{Q}) , \tag{1}$$

where

$$S_{\alpha\beta}(\mathbf{Q}) = \langle A_\alpha^*(\mathbf{Q}) A_\beta(\mathbf{Q}) \rangle . \tag{2}$$

$A_\alpha(\mathbf{Q})$ gives the amplitude of scattering by species α at scattering vector $\mathbf{Q}$:

$$A_\alpha(\mathbf{Q}) = \frac{1}{\sqrt{N_\alpha}} \sum_{j=1}^{N_\alpha} f_\alpha(\mathbf{Q}) e^{i\mathbf{Q}\cdot\mathbf{r}^j} , \tag{3}$$

where $f_\alpha(\mathbf{Q})$ is the appropriate form factor, given in Ref. 20. Since, in the simulations, we employ periodic boundary conditions, we may only calculate the scattering intensity at points which satisfy

$$\mathbf{Q} = \frac{2\pi}{na}(l_x, l_y, l_z) , \tag{4}$$

where a is the unit-cell length of the crystal, n is the number of unit cells along a given direction of the primitive simulation cell ($n = 5$ for $N = 500$ ions, $n = 6$ for $N = 864$, etc.), and l_x, l_y, l_z are integers.

The total scattering contains contributions from the average structure of the systems which is responsible for the Bragg scattering,

$$S^{\text{Bragg}}(\mathbf{Q}) = |\langle A_{\text{Ag}}(\mathbf{Q}) + A_{\text{I}}(\mathbf{Q}) \rangle|^2 , \tag{5}$$

and from diffuse scattering, which is due to thermal and structural disorder,

$$S^{\text{diff}}(\mathbf{Q}) = S^{\text{tot}}(\mathbf{Q}) - \frac{1}{N} S^{\text{Bragg}}(\mathbf{Q}) . \tag{6}$$

Note that Bragg scattering is allowed only at Q values corresponding to the reciprocal-lattice positions for which $l_x + l_y + l_z$ is an even integer, in a bcc crystal. We have calculated the diffuse scattering at 500 K in the planes $(HK0)$ [i.e., $\mathbf{Q} = 2\pi/(na)(H,K,0)$], $(HK1)$, and $(HK2)$, where experimental results are available due to Cava and co-workers.[1]

A comparison between the simulation and experimental results for $(HK0)$ plane is shown in Fig. 1. In general terms, the simulation reproduces the experimental features in a very satisfactory way with the diffuse scattering appearing as [110]-type streaks between neighboring Bragg reflections.[1] Similar good agreement is also found for the $(HK1)$ and $(HK2)$ planes for which we show relief plots in Fig. 2. At this qualitative level the simulation reproduces the ionic disorder as sensed by the scattering experiments.

On closer examination some differences between the experimental and simulation contour plots are apparent. In the experimental data the maxima of the diffuse scattering occur at the Bragg peak positions whereas the maxima in the calculated patterns are slightly displaced from the Bragg positions (compare, for example, the contours in the vicinity of [200] in Fig. 1). These differences could be attributable to the fact that our calculations are performed on a grid of limited resolution because of the periodic boundary conditions. The contours are plotted from a 28×28 grid of data points (taken from a run on 1372 particles) which are then interpolated onto an 84×84 grid. This finer mesh is that illustrated in Fig. 2. Similar plots are found from runs with other (smaller) system sizes and using larger and smaller interpolation meshes. Alternatively, the differences could arise from

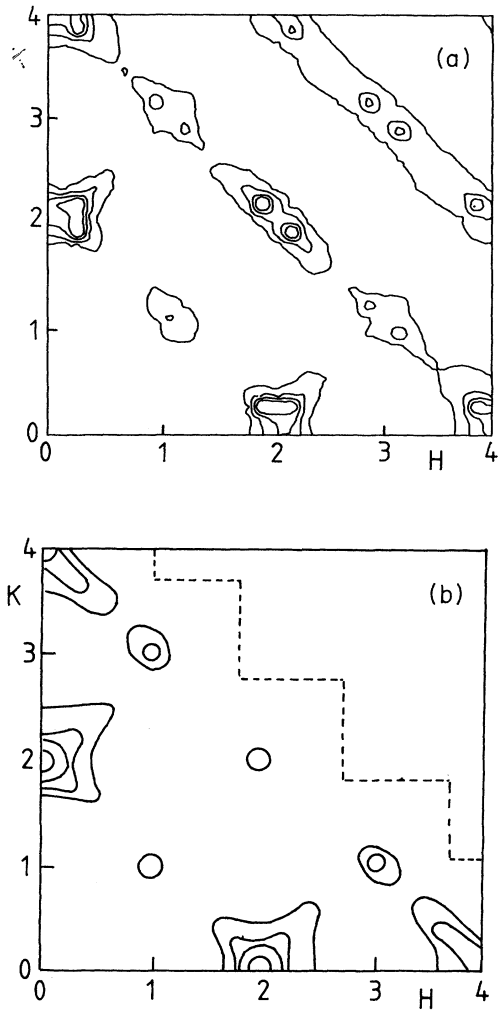

FIG. 1. A comparison of the calculated diffuse x-ray scattering at 500 K from Eq. (6) for the $(H,K,0)$ plane (on the left) with the experimental data of Cava *et al.* from Ref. 1.

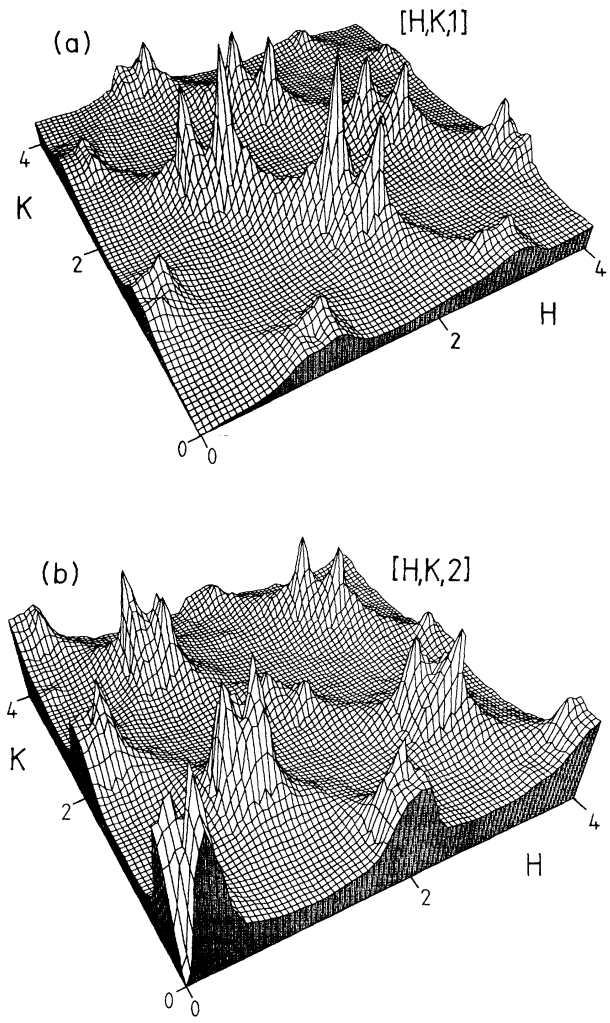

FIG. 2. Relief plots of the calculated diffuse x-ray scattering for the $(H,K,1)$ and $(H,K,2)$ planes at 500 K.

the way that the experimental data is obtained. Since only the total intensity can be observed experimentally, the diffuse scattering close to the Bragg positions must be obtained by extrapolating the diffuse background to the Bragg position. According to the simulation (as best appreciated from Fig. 2), the Bragg position is a local minimum for the diffuse scattering. It is difficult to see how the experimental extrapolation procedure can take this possibility into account.

The simulated total scattering shows numerous features away from the planes which contain the Bragg peaks. In Fig. 3 (lowest curve) we show the total scattering along the direction [111], calculated from the 500 K run. The figure shows quite sharp features away from the Bragg peaks which, at first sight, could suggest that the crystal contains longer-wavelength density modulations than simple bcc. However, these peaks do not arise from a static order because they do not appear in the S^{Bragg}, which measures the average structure of the system. They arise, in fact, from thermal diffuse scattering due to the anomalously soft nature of the phonons of the iodine lattice for certain $\mathbf{K}$ values in the Brillouin zone. For a harmonic crystal, the thermal diffuse scattering may be written[21] as

$$S^{\text{diff}}(\mathbf{Q}) \propto \sum_{\tau} \sum_{j,\mathbf{K}} \delta(\mathbf{Q}+\mathbf{K}-\tau) \frac{|G_j(\mathbf{Q},\mathbf{K})|^2}{\omega_j(\mathbf{K})} , \tag{7}$$

where $\omega_j(\mathbf{K})$ is the frequency of a phonon in branch j with wave vector $\mathbf{K}$, $G_j(\mathbf{Q},\mathbf{K})$ is the amplitude with which it contributes to the x-ray scattering, and τ is the reciprocal-lattice vector. If a phonon with wave vector $\mathbf{K}$ is soft [i.e., $\omega_j(\mathbf{K}) \rightarrow 0$], then peaks will be seen in $S^{\text{diff}}(\mathbf{Q})$ at points where $\mathbf{Q}=\tau+\mathbf{K}$, i.e., as side bands about the Bragg peaks. The structure along the [111] direction can thus be explained as due to a low-frequency

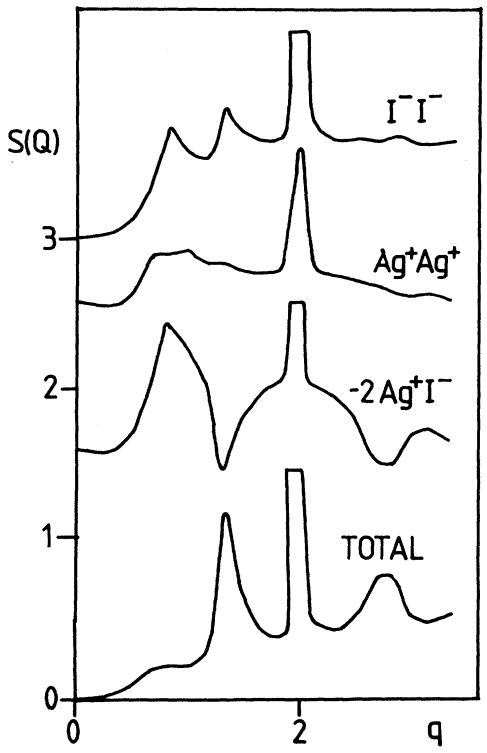

FIG. 3. The total scattering [Eq. (1)] and the partial scattering structure factors along the $\mathbf{Q}=(2\pi/a)(q,q,q)$ direction, where a is the bcc unit-cell side; each plot is vertically offset by one unit which corresponds to $\frac{1}{300}$ of the Bragg-peak height. Note the Bragg peak at $q=2$ and the diffuse scattering peaks at $q\cong 2\pm\frac{2}{3}$ which arise from the "soft" $(2\pi/a)(\frac{2}{3},\frac{2}{3},\frac{2}{3})$ phonon.

phonon with wave vector $(2\pi)/a(\frac{2}{3},\frac{2}{3},\frac{2}{3})$. Since the silver ions are disordered, this motion must be associated with the iodine sublattice.

We have calculated the dynamic structure factor $S(\mathbf{Q},\omega)$ for the I^- ions, i.e.,

$$S(\mathbf{Q},\omega)=\mathrm{Re}\left[\int_0^\infty e^{-i\omega t}\langle A^*_{I^-}(\mathbf{Q},t)A_{I^-}(\mathbf{Q},0)\rangle dt\right], \quad (8)$$

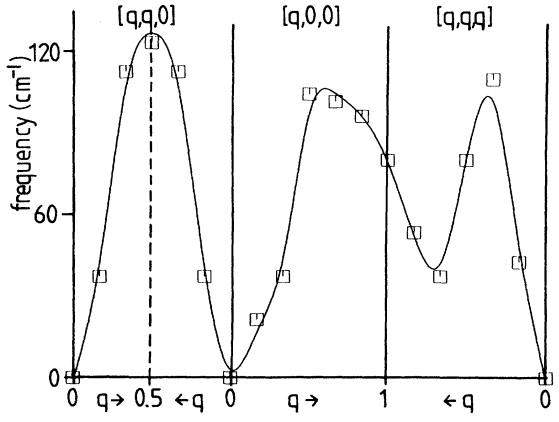

FIG. 4. The phonon dispersion curve for the iodine sublattice calculated from the position of the peaks in the dynamic structure factor for the iodine ions, note the low frequency of the $(2\pi/a)(\frac{2}{3},\frac{2}{3},\frac{2}{3})$ phonon.

in order to examine the longitudinal phonon dispersion curve along the principal directions in reciprocal space. It can be seen from Fig. 4 that the dispersion curve shows a sharp minimum at the $(\frac{2}{3},\frac{2}{3},\frac{2}{3})$ position. This type of phonon behavior is well known in bcc crystals,[22,23] it can be shown by simple geometrical argument that it is a consequence of the fact that the distance between *nn* atoms along the [111] direction does not alter in the longitudinal $(\frac{2}{3},\frac{2}{3},\frac{2}{3})$ motion.

In fact, the oscillation of the iodine sublattice contributes to the diffuse scattering by both the iodine and the silver ions. In Fig. 3 we show the separate contributions $S_{AgAg}(\mathbf{Q})$ $S_{AgI}(\mathbf{Q})$, and $S_{II}(\mathbf{Q})$. The thermal diffuse contribution from the $(\frac{2}{3},\frac{2}{3},\frac{2}{3})$ phonon is evident in the cross term. This implies that the silver ions are able to follow the iodine-ion motion associated with this low-frequency mode. (Note that the period of this phonon mode is roughly 0.16 psec compared to 3 psec for residence time[12] of an Ag^+ ion at a single Td site at 500 K, i.e., the local coordination structure around a given I^- is stable for about five periods of the phonon at this temperature.) We suggest that a detailed experimental study of the temperature dependence of the (TDS) thermal diffuse scattering associated with the $(\frac{2}{3},\frac{2}{3},\frac{2}{3})$ phonon would be a useful way of studying the correlation between the iodine and silver motion.

The motivation for Cava's diffuse-scattering study was to try to see the structure associated with the positional correlations between the silver ions. In fact, the x-ray diffuse scattering is dominated by thermal diffuse scattering. An *elastic* diffuse neutron study is necessary to obtain the structural information.

IV. LIGHT-SCATTERING ANALYSIS

The experimental results on the Raman spectra have been summarized in the introduction to the paper by

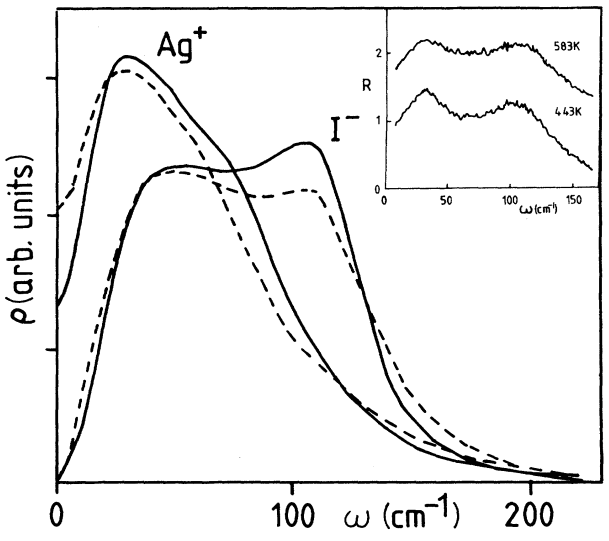

FIG. 5. The "density of states" (i.e., the spectral density of the velocity autocorrelation function) of the iodine and silver ions at 500 K (solid lines) and 900 K (dashed). The Bose-factor-reduced Raman spectra of α-AgI, from Refs. 8, 17, and 18, are shown in the inset.

Mazzacurati *et al.*[18] From two wave numbers upwards, the shapes of the polarized $Z(YY)Z$ and depolarized $Z(XY)Z$ spectra are the same and closely related to the one-phonon density of states (DOS) of the I^- sublattice. This similarity emerges when the observed spectra $I_{AB}(\omega)$, where A and B denote the polarizations of the incident and scattered radiation ($A=B=Y$ is polarized scattering, and $A=X$, $B=Y$ is depolarized) are reduced $[R_{AB}(\omega)]$ by removal of the Bose factor

$$R_{AB}(\omega)=\frac{I_{AB}(\omega)}{n(\omega)+1} . \tag{9}$$

The silver and iodine "densities of states" are obtained from simulation as the spectral densities of the velocity autocorrelation functions of the ions,

$$\int_0^\infty e^{-i\omega t}\langle \mathbf{v}^i(t)\cdot\mathbf{v}^i(0)\rangle dt=\rho(\omega) , \tag{10}$$

where $\mathbf{v}^i(t)$ is the velocity of ion i.[24] Results at 500 and 900 K are shown in Fig. 5. The experimental reduced Raman spectra at 443 and 583 K are shown as an inset.

Mazzacurati *et al.*[17,18] have interpreted the observation that the light-scattering spectrum resembles the iodine DOS to mean that the I^- ions act as incoherent scattering centers. The silver ions induce a change in the polarizability of each I^- ion whose value depends upon the local configuration of the silver ions. This induced polarizability has a random component because of the disorder of the local configurations, and hence the scattering is incoherent. The scattering by the silver ions themselves is much smaller due to the lower cation polarizability and is expected to occur at low frequency. This mechanism may be summarized in the following equations. The light-scattering spectra are given by

$$I_{AB}(\omega)=\lim_{\mathbf{k}\to 0}\int_0^\infty e^{-i\omega t}\left\langle \sum_l \alpha^l_{AB} e^{i\mathbf{k}\cdot[\mathbf{R}^l+\mathbf{u}^l(t)]}\sum_j \alpha^j_{AB} e^{i\mathbf{k}\cdot[\mathbf{R}^j+\mathbf{u}^j(0)]}\right\rangle dt , \tag{11}$$

α^i_{AB} is a component of the instantaneous value of the polarizability of iodine ion i, $\mathbf{R}^i$ is the equilibrium lattice position of ion i, and $\mathbf{u}^i$ is the instantaneous displacement, and the sum runs only over the iodine ions (because the silver contribution is presumed negligible). $\mathbf{k}$ is the scattering vector of the light and the $\mathbf{k}\to\mathbf{0}$ limit is appropriate because of the long wavelength of the light.

The polarizability consists of an average value α and a fluctuating part ξ^i, induced by interaction with the silver ions,

$$\alpha^l_{AB}=\bar{\alpha}\delta_{AB}+\xi^l_{AB} , \tag{12}$$

where δ_{AB} is the Kroïecker δ. The expression for the light-scattering spectrum[25] then becomes

$$I_{AB}=\lim_{k\to 0}\int_0^\infty e^{-i\omega t}\left[\bar{\alpha}^2\delta_{AB}\left\langle\sum_{l,j} e^{i\mathbf{k}\cdot[\mathbf{u}^l(t)-\mathbf{u}^j(0)]}e^{i\mathbf{k}\cdot(\mathbf{R}_l-\mathbf{R}_j)}\right\rangle+\left\langle\sum_{l,j}\xi^l_{AB}(t)\xi^j_{AB}(0)e^{i\mathbf{k}\cdot[\mathbf{u}^l(t)-\mathbf{u}^j(0)]}e^{i\mathbf{k}\cdot(\mathbf{R}_l-\mathbf{R}_j)}\right\rangle\right]dt , \tag{13}$$

where we have neglected terms which are odd in ξ^i. The first term will contribute as Brillouin scattering associated with acoustic phonons of wave vector $\mathbf{k}$ if the lattice symmetry permits.[26] This will occur at very low frequency. Our concern is the "Raman" scattering from the second term. This will reflect the relative motion of the silver and iodine ions through the time dependence of $\xi^l_{AB}(t)$. We may simplify this term by noting that any correlation which exists between the $\xi^i_{AB}(t)$'s will be much shorter range than k^{-1} so that both exponential factors may be replaced by unity,

$$I^{\text{Raman}}_{AB}\simeq\int_0^\infty dt\, e^{-i\omega t}\left\langle\sum_{i,j}\xi^i_{AB}(t)\xi^j_{AB}(0)\right\rangle . \tag{14}$$

If, in fact, the values of the $\xi^i_{AB}(t)$ on different sites are completely uncorrelated, the spectrum will become "incoherent,"

$$I^{\text{Raman}}_{AB}\simeq\frac{N}{V}I^{\text{inc}}_{AB}=\frac{N}{V}\int_0^\infty dt\, e^{-i\omega t}\langle\xi^1_{AB}(t)\xi^1_{AB}(0)\rangle . \tag{15}$$

The Bose-factor reduced incoherent spectrum may be related to the density of states in the following way: we note that, at low frequency,

$$R^{\text{inc}}_{AB}(\omega)\simeq\frac{\omega\hbar}{k_BT}I^{\text{inc}}_{AB}(\omega)=\frac{-\hbar}{k_BT\omega}\int_0^\infty e^{-i\omega t}\frac{\partial^2}{\partial t^2}\langle\xi^1_{AB}(t)\xi^1_{AB}(0)\rangle dt . \tag{16}$$

The induced polarizability of an iodine ion will depend on the distance between the neighboring silver ions so that

$$\frac{\partial}{\partial t}\xi^1_{AB}(t)=\sum_\nu(\mathbf{v}_1-\mathbf{v}_\nu)\cdot\frac{\partial}{\partial\mathbf{r}_{1\nu}}\xi^1_{AB}(t) , \tag{17}$$

where the sum over ν runs over the Ag^+ neighbors of iodine 1 and the $\mathbf{r}_{1\nu}$ are their positions relative to the iodine ion. Consequently, we may write

$$R^{\text{inc}}_{AB}(\omega)\propto\frac{N}{k_BT\omega}\int_0^\infty e^{-i\omega t}\left\langle\sum_\nu[\mathbf{v}_1(t)-\mathbf{v}_\nu(t)]\cdot\frac{\partial}{\partial\mathbf{r}_{1\nu}}\xi^1_{AB}(t)\sum_\mu[\mathbf{v}_1(0)-\mathbf{v}_\mu(0)]\cdot\frac{\partial}{\partial\mathbf{r}_{1\mu}}\xi^1_{AB}(0)\right\rangle . \tag{18}$$

For this expression to reduce to the iodine density of states, as suggested by Mazzacurati *et al.*,[17,18] it is necessary for the only significant frequency dependence to arise from the iodine velocity correlations, i.e., the silver ions are to be considered stationary on the time scale of interest and the time dependence of $\xi^1_{AB}(t)$ is to be neglected. We would then obtain

$$R^{\rm inc}_{AB}(\omega) \propto \frac{1}{\omega}\rho(\omega) , \tag{19}$$

which is the result obtained by Mazzacurati *et al.*[17,18] Similar approximations have been used to discuss the shapes of Raman spectra of liquids.[27]

It is of interest to use the simulation to see to what extent this sequence of approximations may be justified. In order to do this we need a model for the interaction-induced polarizability. Recently interaction-induced polarizabilities in ionic crystals have been studied using *ab initio* electronic structure calculations,[28,29] and the spectrum calculated from them, using simulation methods, shown to be in quantitative agreement with the experimental Raman spectra for the lighter alkali halides.[29,30] Unfortunately, we cannot carry out this type of calculation for AgI as the ions contain too many electrons. However, we can make use of the conclusions of the alkali-halide studies, in a qualitative way, to guide us in the development of a useful model. It is found that the spectral shape is dominated by a short-range, interaction-induced contribution to the anion polarizability. This may be represented, for the reasons discussed in Ref. 29, by the form

$$\alpha^i_{AB} = [(\underline{K}^i)^{-1}]_{AB} , \tag{20}$$

where

$$K^i_{\alpha\beta} = K_0\delta_{\alpha\beta} + \sum_{i\in \mathrm{Ag}^+} A(r^{ij})\delta_{\alpha\beta} + \sum_{i\in \mathrm{Ag}^+} B(r^{ij})\{3\hat{\mathbf{r}}^{ij}_\alpha \hat{\mathbf{r}}^{ij}_\beta - \delta_{\alpha\beta}\} . \tag{21}$$

The model represents the anion polarizability as the inverse of a force-constant matrix (as in the Drude model of the polarizability). The force constant depends on the positions of the neighboring Ag^+ ions. This reflects the resistance to the polarization of the electron cloud due to the confinement by the local coordination of the cations about the anions.[28] The functions A and B control the isotropic and anisotropic fluctuations in this confining potential. These functions are short ranged, so that only the first coordination shell of cation neighbors contributes to the interaction-induced polarizability of the anion. For the AgI calculations we used

$$A(r_{ij}) = 0.0024e^{-(r_{ij}-\sigma)/0.5706} , \tag{22}$$

$$B(r_{ij}) = 0.002\,03e^{-(r_{ij}-\sigma)/0.6061} , \tag{23}$$

where the numerical values are in atomic units (a.u.). We take σ, the Ag^+-I^- interionic separation, to be just smaller than the first peak in the Ag^+-I^- pair-distribution function, where we find a value of 2.4 Å, and $K_0 = 0.033\,27$ (a.u.)$^{-1}$. The values of the prefactors and exponents are the ones used to represent the Cl^- ion polarizability in NaCl.[30] The polarizability model is not being used in an attempt to specifically model the AgI behavior, rather as a physically reasonable generic model for the anion polarizability which we can use to judge the validity of the approximations introduced to relate the light-scattering spectra to the iodine DOS.

We have calculated the three independent contributions (in a cubic crystal[26]) to the light-scattering spectrum, $I^{\rm Raman}_I(\omega)$, $I^{\rm Raman}_{A_1}(\omega)$, and $I^{\rm Raman}_{A_2}(\omega)$, [see Eq. (14)]. The isotropic scattering, $I^{\rm Raman}_I$ is caused by fluctuations in the trace of $\underline{\xi}^i$, the diagonal anisotropic term $I^{\rm Raman}_{A_1}$ by the fluctuations in $\xi^i_{YY} - \frac{1}{3}\mathrm{tr}\underline{\xi}^i$, and the off-diagonal anisotropic term $I^{\rm Raman}_{A_2}$ by ξ^i_{XY}. The isotropic spectrum reflects the breathing motion of the cation coordination shell, whereas the anisotropic spectra reflect changes in its shape. We have also calculated their incoherent counterparts, from Eq. (15), and the Bose-reduced spectra $R^{\rm Raman}_I(\omega)$, $R^{\rm inc}_I(\omega)$, etc.

With these spectra we can examine the approximate relationship in Eq. (15), which rests on the assumption that the local silver configurations about different iodines are uncorrelated. The full Raman spectra and their incoherent counterparts are compared in Figs. 6 and 7. The full Raman spectra are considerably noisier than the incoherent ones (as is normally the case for collective correlation functions); they contain small bumps which are due purely to poor statistics. Within this limitation, however, it can be seen that Raman and incoherent spectra resemble each other quite closely, both in overall shape and in intensity. The simulation results with the model polarizability support the approximation in Eq. (15).

The reduced anisotropic spectral shapes agree extremely well with the experimental ones (see inset to Fig. 5). Both the low- and high-frequency bumps are found at the correct frequencies and the relative intensities change with temperature in qualitatively the same way as found experimentally. It would seem that the *ad hoc* polarizability model we have used does contain the important factors which determine the line shape. However, not surprisingly, the relative intensities of the $I^{\rm Raman}_I(\omega)$, $I^{\rm Raman}_{A_1}(\omega)$, and $I^{\rm Raman}_{A_2}(\omega)$ are not in accord with the experiment, as we shall see.

We may also compare the simulated spectrum with the suggestion of Mazzacurati *et al.*[17,18] that the reduced spectrum should resemble the iodine density of states divided by frequency [Eq. (19)]. In fact, the simulated reduced spectrum is seen to be much closer to the iodine DOS itself, as may be seen from Fig. 5. The high-frequency bump can be recognized immediately, but when the DOS is divided by frequency [Eq. (19)], the amplitude of the low-frequency bump becomes far more prominent than is seen in either the simulated or experimental reduced spectrum.

As stated above, in order to obtain Eq. (19) we must apply some severe approximations to Eq. (18). The silver-ion motion must be neglected as must cross correlations between the silver and iodine velocities. In fact, as Fig. 5 shows, the silver-ion DOS has its maximum in

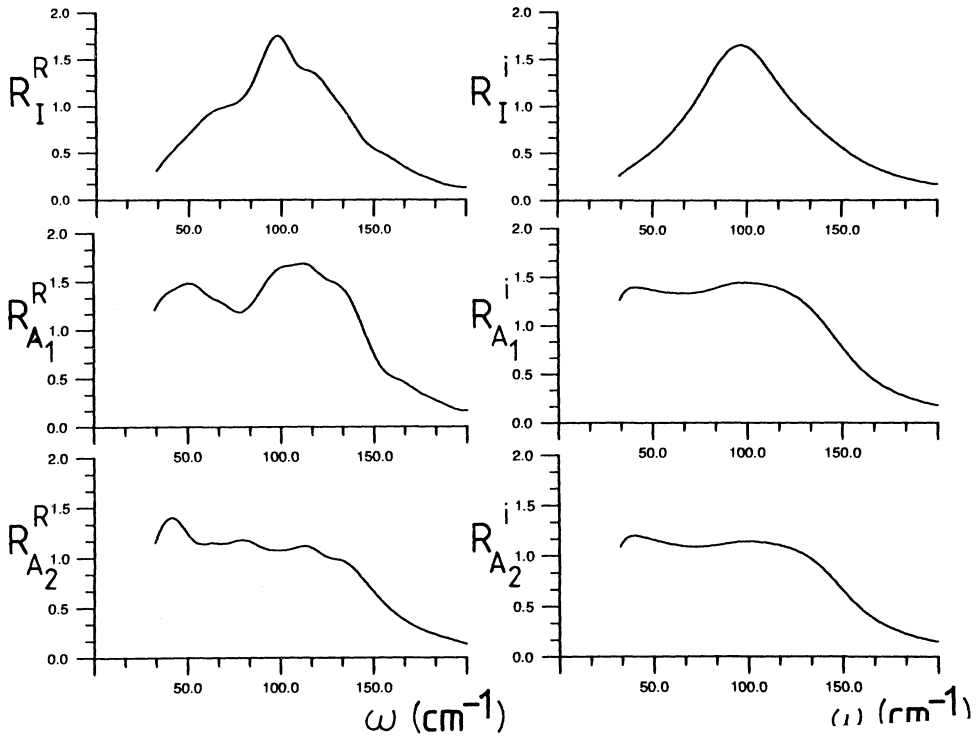

FIG. 6. The Bose-factor-reduced Raman (R_I^R, $R_{A_1}^R$, and $R_{A_2}^R$) spectra at 500 K are compared with their incoherent counterparts (R_I^i etc.); the vertical scales are arbitrary but common to all the plots.

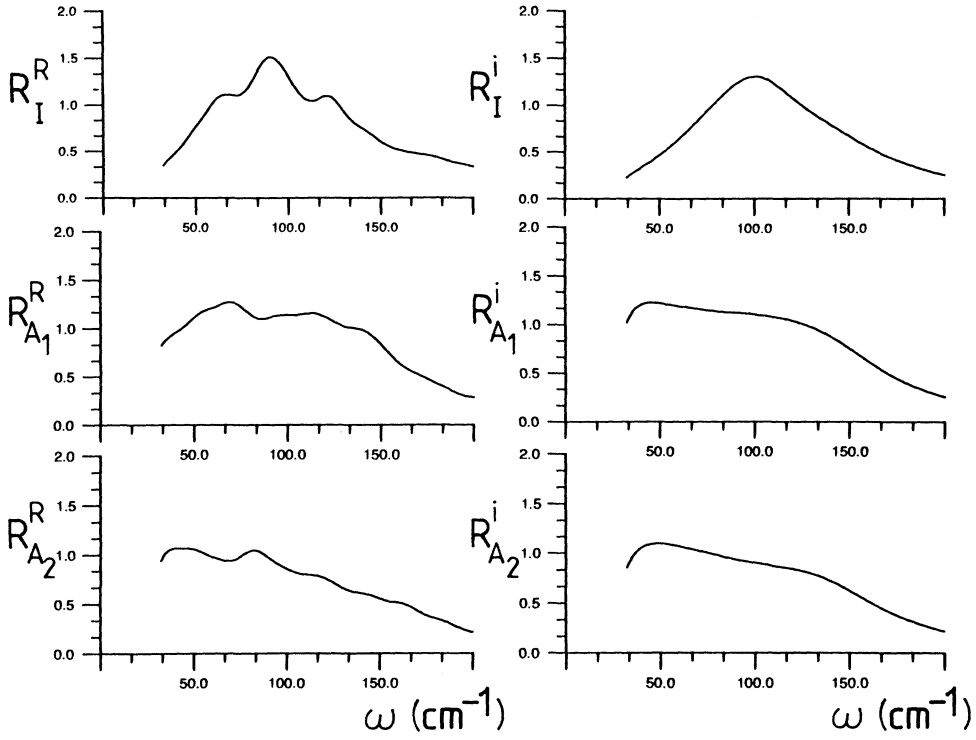

FIG. 7. The Bose-factor-reduced Raman (R_I^R, $R_{A_1}^R$ and $R_{A_2}^R$) spectra at 900 K are compared with their incoherent counterparts (R_I^i etc.); the vertical scales are arbitrary but common to all the plots.

the same frequency range as the low-frequency bump in the iodine DOS—showing that the silver-ion motion cannot be neglected in discussing the spectrum in this regime. A better model for the shape of $R_{AB}^{\rm inc}(\omega)$ at low frequency might be to assume that the motion of an iodine ion is highly correlated with that of its silver neighbors, the silver ions are able to follow the *low-frequency* iodine motions (cf. the discussion of the thermal diffuse x-ray scattering), resulting in a small *relative* velocity. In this way, the amplitude of the reduced spectrum at low frequency predicted by Eq. (18) would be lower than that predicted by the iodine DOS alone. At high-frequency the silver ions are unable to follow the velocity fluctuations of their neighboring iodine and the neglect of the silver-ion motion is appropriate.

V. LIGHT SCATTERING: INTENSITY AND POLARIZATION RATIO

The isotropic and anisotropic spectrum are related to the observed polarized and depolarized ones by

$$I_{YY}(\omega)=I_I(\omega)+\tfrac{4}{3}I_{A_1}(\omega) \tag{24}$$

and

$$I_{XY}(\omega)=I_{A_2}(\omega)\ . \tag{25}$$

Experimentally, it is found that the depolarization ratio (I_{XY}/I_{YY}) is frequency independent (from 20–200 $\rm cm^{-1}$ and very large, having a value of 1 at low temperature to 0.7 near the melting point).[17] As we have seen from the simulation, the isotropic spectrum appears to have a different shape to the ansiotropic ones, which are quite similar. Hence, the only way the depolarization ratio can be frequency independent and as large as observed is if the intensity of the isotropic spectrum is much lower than that of the anisotropic ones. This is not the case for the *ad hoc* polarizability model, as Figs. 6 and 7 show. However, the model could easily be adjusted to bring the predictions into better agreement with experiment; reducing the amplitude of the (breathing) $A(r_{ij})$ factor relative to the $B(r_{ij})$ will bring about a corresponding reduction in the intensity of the isotropic spectrum relative to the anisotropic without compromising the good agreement of shape. With this modification, the calculated depolarization ratio reflects the ratio of the two anisotropic spectra and becomes roughly constant, with a value of 0.7 at 500 and 900 K. This value is lower than the experimental value at 500 K. The two anisotropic spectra reflect fluctuations of different symmetry in the local coordination structure around the anion. In I_{A1} we see the fluctuations (of E_g symmetry) in $\xi_{YY}^i-\frac{1}{3}\mathrm{tr}\underline{\xi}^i$, i.e., deformations along the [010] direction (towards the face of the cubic cell in which each I^- is located). In I_{A2} we see the (T_{2g} symmetry) fluctuations in ξ_{XY} caused by deformation along the [110] direction. The similar shapes of $R_{A_1}(\omega)$ and $R_{A_2}(\omega)$ (in experiment and simulation) show that these fluctuations are dynamically equivalent. Their roughly equal intensities in the simulation (Figs. 6 and 7) suggest that the probability of the two types of fluctuation are roughly equal in the simulated structures at both 500 and 900 K (i.e., fluctuations in all directions are equally likely). However, the magnitude of the experimental depolarization ratio behaves somewhat differently. At low temperatures it takes on a value close to unity. This shows that $I_{A_2}\simeq\frac{4}{3}I_{A_1}$ and suggests that the T_{2g} fluctuations are slightly more probable. Between 650 and 700 K the depolarization ratio shows a rapid drop from 1 to 0.7 (i.e. the simulation value) at which it remains up to the melting point. It is possible that the discrepancy between the experiment and the simulation with regard to the depolarization ratio is due to the polarizability model, or it could be that the different amplitudes of the E_g and T_{2g} fluctuations reflect an aspect of the silver-ion motion which is not reproduced in the simulation.

The change in depolarization ratio found in the experiments is accompanied by a sharp decrease in the intensities of the reduced spectra.[2,17] As is clear from Figs. 6 and 7, the calculated spectra do not show this behavior. We believe that the fact that we have found a roughly constant depolarization ratio and intensity over a range of temperature in which this quantity exhibits significant changes in the experiments could be connected to the fact that we carried out the simulations at constant density. Tallon's simulations show that the density we have used would correspond to a very high pressure at the temperature at which the Raman and heat-capacity anomalies are observed.[11] Further investigations on this point are currently underway.

VI. LIGHT SCATTERING AND THE SILVER-ION DISORDER

In order to explain the temperature dependence of the Raman intensity and depolarization ratio, Mazzacurati *et al.*[8,18] considered various possible local configurations of the silver ions and the way in which they could contribute to the spectra. In our terms, they sought to account for the amplitude of the fluctuations of different symmetry through the introduction of several distorted coordination structures.

An ideally coordinated I^- ion (four silver teterahedrally disposed around the iodine) simply has the mean polarizability and hence does not contribute to the spectra. It was shown that two possible distorted configurations involving three- and five-fold coordination of silver around iodine could cause large changes in the off-diagonal elements of $\underline{\xi}$ and, hence, give rise to a depolarized spectrum. A simple model for the energy of these defects suggested that they are thermally accessible. The temperature dependence of the intensity and depolarization ratio was therefore explained as a rapid decrease of the number of 3 and 5 coordinated iodines between 650 and 700 K. In order to account for the counterintuitive idea that the number of "defects" decreases as the temperature increases, it was suggested that the 3- and 5-coordinate iodines might be involved in some kind of cooperative interaction. Since 700 K is also the temperature at which the heat-capacity anomaly was observed,[16] it was argued that these phenomena might be linked.

We have examined this idea in the computer simula-

tion. The coordination number p_i of the I^- ion is found from

$$p_i = \sum_{j \in Ag^+} e^{-[(r^{ij}-\sigma)/\Delta]^8}, \tag{26}$$

where $\sigma = 2.7$ Å and $\Delta = 1.2$ Å. The exponential function gives a number very close to one if j is within a coordination shell of iodine (i.e., lies within the first peak of the iodine silver pair-distribution function) and zero outside. It has the advantage over a step function of being continuous and reflects the fact that cases of intermediate coordination do exist. An I^- ion is defined as being 3 coordinate if $2.5 \leq p_i \leq 3.5$ etc., the average number of such ions is n_3. With this definition and the choices for σ and Δ given above, the average value of p_i is 4, to two significant figures, and the numbers of 3- and 5- coordinate ions are roughly equal.

Contrary to the suggestion of Mazzacurati *et al.*, the number of coordination defects increases with increasing temperature between 500 and 900 K. We note once again that our simulations were carried out at constant density, but it seem likely that lattice expansion could only increase the number of defects further. A plot of $\ln([n_3+n_5]/2n_4)$ versus $1/T$ (Fig. 8) gives the free energy for the formation of a 3 and 5 coordinate defect pair as $840k_B$, where k_B is Boltzmann's constant.

The concentration of coordination defects in the crystal is quite high; we have investigated the possibility that they are spatially correlated by calculating pair-distribution functions for the I^- ions with different coordination numbers, e.g., $g^{35}(r)$ gives the probability that a 5-coordinate iodine will be found distance r away from a 3-coordinate iodine ion. Note that these defects are oppositely charged and might be expected to attract each other. Because of the lattice structure, $g^{35}(r)$ is a highly oscillatory function and it is preferable to display the normalized function $g^{35}(r)/g^{44}(r)$, where $g^{44}(r)$ is the I^- distribution function for the ideal fourfold coordination. The departure of this normalized function from unity is a measure of the degree of correlation in the position of the defects.

In Fig. 9 we show the function $g^{35}(r)/g^{44}(r)$ at different temperatures. These functions show a weak correlation at short range. Much of this is associated with the deformation of the lattice on formation of the defects, giving the "derivative shape" apparent at about 5 Å. The interaction of the defects does not seem to be very strong, and does not extend beyond two or three lattice parameters.

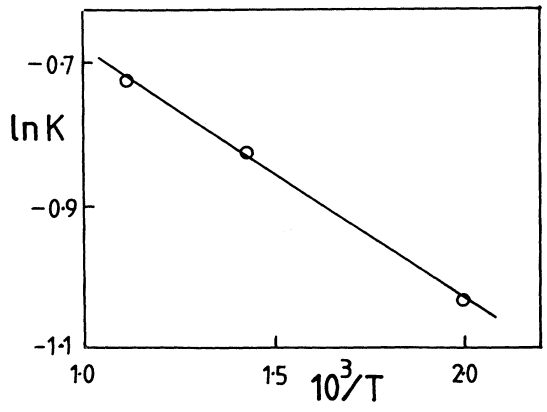

FIG. 8. A semilogarithmic plot of $K = (n_3+n_5)/2n_4$, where n_i gives the mean number of iodine ions with i silver-ion neighbors vs $1/T$; the slope gives the free energy for creation of a coordination defect.

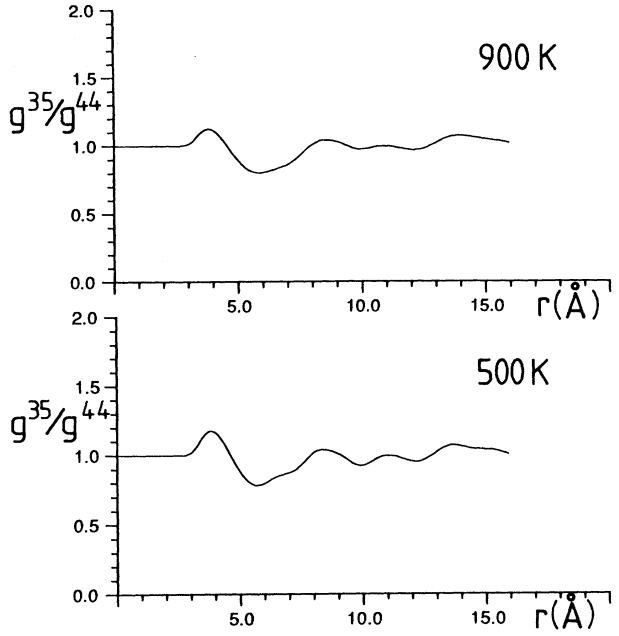

FIG. 9. Reduced radial distribution function for 3- and 5-coordinate iodine ions; the bcc unit-cell side is 5.2 Å.

VII. LATTICE-GAS MODEL

Szabó[7] has examined the disorder from the viewpoint of the silver-silver correlations, rather than by consideration of the coordination structure around iodine. The silver ions are regarded as tied to the tetrahedral sites, which do not form a Bravais lattice but may be regarded as forming six interpenetrating bcc sublattices. The locations of the Td sites within the unit cell are indicated in Fig. 10. There are 12 sites wholly within the cell, which contains two Ag^+ ions on the average, so that each sublattice is only $\frac{1}{6}$ occupied if the Ag^+ ions are randomly disposed. The sublattices are labeled 1–6. As indicated in Fig. 10, points on sublattice 1 have nearest-neighbor (NN) sites on sublattices 2, 3, 5, and 6, and next-nearest-neighbor (NNN) sites on sublattice 4. Initially the sublattice occupancy at finite temperature was studied with a lattice-gas, mean-field theory. Many possible phases were identified, some of which involved preferential occupation of certain sublattices.[7(a)].

Szabó and Kertész[7(b)] have subsequently performed a Monte Carlo calculation on a model with direct NN and NNN interactions between occupied lattice points, with longer-range interactions included via a mean-field term. They showed that, for a certain choice of interaction pa-

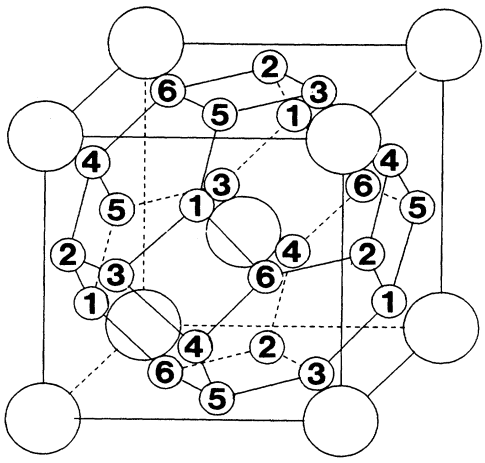

FIG. 10. The labeling of the "tetrahedral" interstitial sites of a bcc lattice, as given by Szabó (Ref. 7). Note that sites with a given label form a bcc sublattice and that sites of types 2, 3, 5, and 6 are nearest neighbors of site 1 and that site 4 is a next-nearest neighbor.

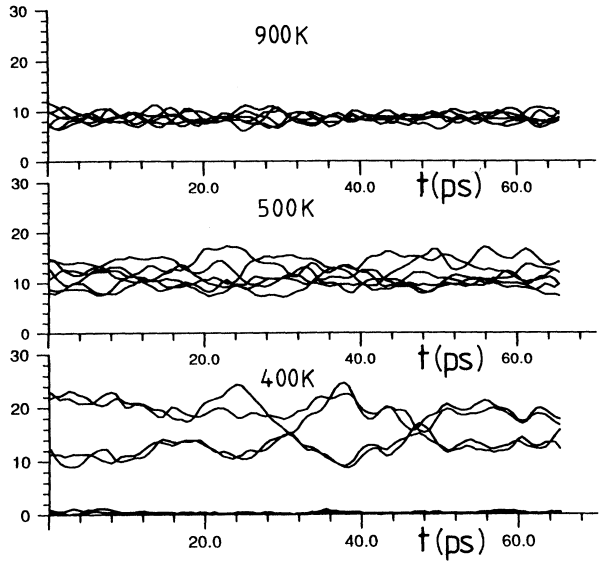

FIG. 11. Instantaneous percentage occupation numbers for each of the six Szabó sublattices at three different temperatures. Note that, in the low-temperature data, two sublattices are unoccupied.

rameters, different phases could be stable as the temperature was changed: *A*, an ordered low-temperature phase in which one sublattice is predominantly occupied, *B*, a disordered high-temperature phase in which the sublattice occupancies are equal, and *C* an intermediate phase in which two sublattices (which involve no NN interactions) are predominantly occupied (e.g., sublattices 1 and 4 in the figure). The authors showed that phase *C* was stable only in the presence of the long-range, mean-field term in the Hamiltonian.

In the simulation, Ag^+ ions are assigned to the tetrahedral site sublattices in the following way. A coordinate system registered with the I^- lattice is found and the unit cell which contains a given Ag^+ ion is identified. The Td sites occur at $(\frac{1}{4},0,\frac{1}{2})$ and at all symmetry-related points in the cell. An Ag^+ ion is said to sit in a given Td site if it lies within a cube of side $a/4$, centered on that Td location. Despite this rather generous criterion for site occupancy by no means are all the Ag^+ ions allocated to Td sites. At 500 K, only 70% are allocated, and this number becomes lower at higher temperatures (with our criterion, the Td sites occupy $\frac{3}{16}$ unit-cell volume). This is consistent with previous simulation and experimental findings that Ag^+ ions are not tightly located at any site within the crystal. Nevertheless, we will persist with an analysis in terms of intersitital site occupancy, discarding the unallocated ions, in order to make contact with the Szabó analysis and to understand the influence of the underlying I^- lattice on the Ag^+-Ag^+ positional correlations.

In Fig. 11 we show the instantaneous percentage of Ag^+ ions found on each Td site sublattice type as a function of time throughout the 900, 500, and 400 K simulation runs. The average occupation numbers allow us to judge the possibility that the system as a whole has condensed into either phase *B* or phase *C*. At 900 and 500 K, the average sublattice occupations are equal, but at the lower temperature the fluctuations of the individual sublattice occupations from this average value become larger and persist for longer. At 400 K the sublattice occupations are unequal with two sublattices unoccupied, suggesting that an ordering transition of the Ag^+ ions has taken place. We will discuss this phenomenon in more detail elsewhere.[31] Here we simply note that the I^- ions in this calculation are in a bcc structure, the $\alpha \rightarrow \beta$ transition (which should occur at about 470 K in the simulation[10,11] is inhibited in our calculations by the cubic periodic boundary conditions. This ordering process must be driven by the Ag^+-Ag^+ interactions; the size and persistance of the fluctuations at 500 K suggest that it is already appreciable well within the α phase.

To examine this process, we have calculated pair-distribution functions for the occupied sites. We define $G^{12}(r)$ to be the probability that if a site belonging to sublattice 1 is occupied, a site of sublattice 2 at a distance r away is also occupied. Of course, r takes on only discrete values determined by the lattice structure. $G^{12}(r)$ is normalized in such a way as to go to unity at long range. Referred to a site of type 1, there are three types of distribution functions (see Fig. 10) not related by symmetry: $G^{11}(r)$, $G^{14}(r)$, and

$$G^{12}(r)=G^{13}(r)=G^{15}(r)=G^{16}(r) \ .$$

All the $G^{ij}(r)$'s referred to other sites are equivalent to one of these three different distribution functions. In the following we will refer to the generic distribution functions as $G^{11}(r)$, $G^{12}(r)$, and $G^{14}(r)$.

Results for this quantity at 500 and 900 K are shown in Fig. 12. The overall appearance suggests a significant degree of positional correlation at the Ag^+ ions extending up to almost two unit-cell lengths with NN and NNN al-

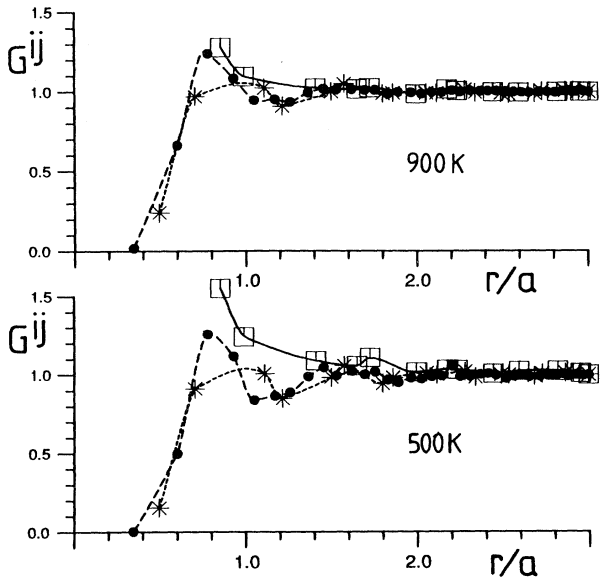

FIG. 12. Partial radial distribution functions for the Szabó sites G^{ij} giving the probability that, if a site of type 1 at the origin is occupied, a site of type 1 (squares), type 4 (stars), or type 2, 3, 5, or 6 (circles) distance r away is also occupied. The function is only defined on the lattice, the lines have been provided to aid the eye.

most unoccupied. The degree of correlation (as witnessed by the height of the first "peak") decreases significantly with increasing temperature. At first sight the correlation appears liquidlike. The different $G^{ij}(r)$ appear to reflect a single distribution function $G(r)$ taken at the different intersite distances which are allowed. In fact, this is not so. For example, in the region of r between 0.8 and 1.4 in the 500 K plot it can be seen that the values of $G^{12}(r)$ and $G^{14}(r)$ are clearly lower than the values of $G^{11}(r)$. This difference is much reduced at the higher temperature. The overall effect of this positional correlation is that the occupation of a given sublattice at one point causes a considerably enhanced probability that nearby ions will occupy the *same* sublattice. This effect is shown in Fig. 13 where we plot the quantities

$$N^{ij}(r)=\frac{\sum_{r'\le r}G^{ij}(r')n^{ij}(r')}{\sum_{r'\le r}n^{ij}(r')}-1\ , \tag{27}$$

where $n^{ij}(r)$ is the number of sites of type j at a given distance from a site of type i. This quantity gives a measure of the excess population of sublattice j around an occupied site of type i. It can be seen that this excess extends out to significant distances, especially at 500 K. The observation that the excess population is on the same sublattice and that the excess is growing as the temperature is reduced suggests that the Ag^+ ions are moving towards Szabó's ordered phase A at low temperature.

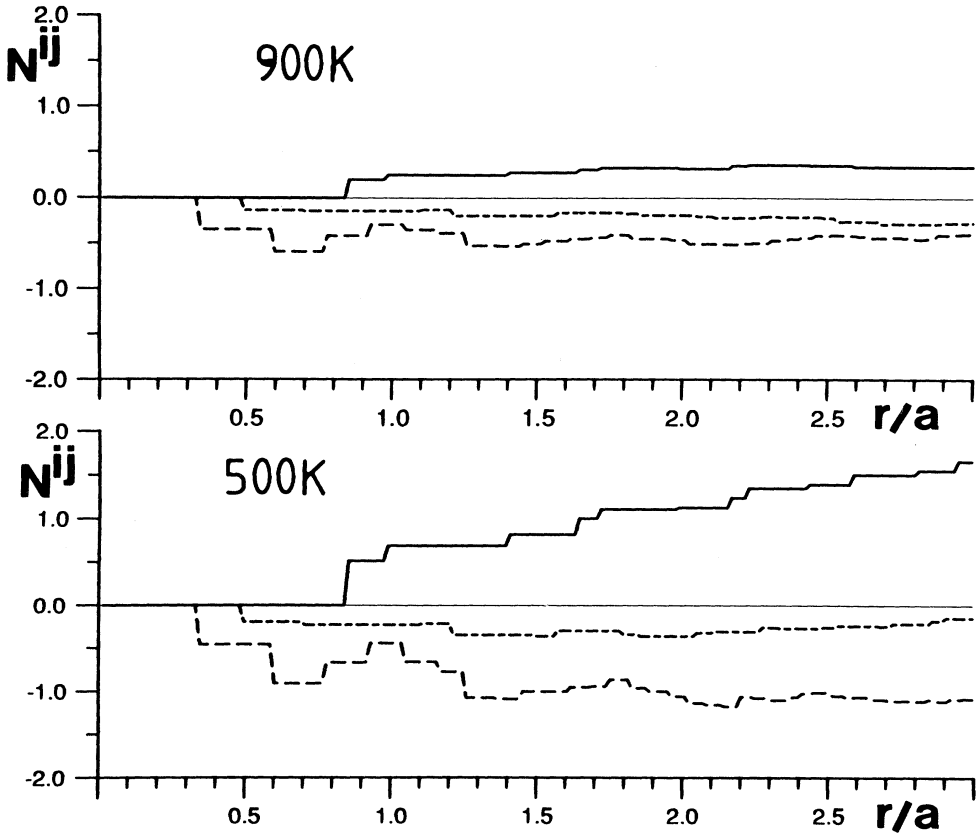

FIG. 13. The excess coordination number [eq. (26)] of sites of type j around a site of type i at the origin. The solid curve is for $i=1, j=1$; the dashed curve is for $i=1, j=2$, 3, 5, or 6, and the dotted curve is for $i=1, j=4$.

However, the appearance of the 400 K data in Fig. 11 shows that what actually occurs is somewhat more complex.

VIII. CONCLUSION

This work has been concerned with the nature of the silver-ion order in simulations of α-AgI at a constant density (corresponding roughly to the experimental density at the α-β phase transition to zero pressure). Given the successes of the RVP potential on other problems, in particular, with the α-β phase transition, we expect the results to give a good guide to the behavior of the real material. The only experiment which clearly reflects the silver-ion disorder is the Raman scattering; the diffuse x-ray scattering seems to be too strongly affected by thermal diffuse scattering for the Ag^+-Ag^+ correlation to show through. Unfortunately, we have no reliable model for the interaction-induced polarizability in order to directly calculate the Raman scattering from the simulation. We have made some progress with an *ad hoc* polarizability model; we were able to reproduce the experimental line shape and to comment on the validity of several approximations used in the analysis of the spectrum. However, we were not able to reproduce the high value of the low-temperature depolarization ratio nor the temperature dependence of the depolarization ratio and intensity. This failure could reflect upon the shortcomings of the model, or that, by working at constant density, we have simply missed the order-disorder transition which the experimental data appears to indicate. It is also possible that the RVP potential does not predict such a transition, but Tallon's findings[11] provide evidence that it does. We are presently trying to find a better polarizability model which will be used at a wider range of statepoints.

Notwithstanding our present inability to connect simulation and real data, we have examined two models for the silver-ion disorder in the lattice. We examined the number of iodine ions with coordination defects, in the sense of a deficiency or excess of coordinated silver ions from the average value of four. We found that the number of these defects increased with temperature and that the defects were at most only weakly spatially correlated, contrary to suggestions made by Mazzacurati *et al.*[18] in their model for the Raman data. We also looked at the positional correlations of the silver ions in the sense suggested by Szabó[7] by analyzing the way the sublattices of tetrahedral sites were occupied. This viewpoint threw up a number of interesting features.

At temperatures greater than 500 K, the silver ions were uniformly distributed over the sublattices (contrary to the suggestion that there might be phase transitions between phases of intermediate silver-ion order within the α phase). The ions did, however, show a tendency to cluster locally on a single sublattice, the strength and range of this correlation increasing as the temperature decreased. It is interesting to speculate that this ordering process might be linked to the $\alpha \rightarrow \beta$ transition which is known to occur with the RVP potential if noncubic periodic boundary conditions are allowed. In our simulations, the iodine ions continue to form a bcc lattice as the temperature drops below the α-β transition temperature, but the silver ions appear to undergo a continuous transition to an ordered state. We are presently investigating this behavior in more detail.[31]

[1] R. J. Cava, R. M. Fleming, and E. A. Reitman, Solid State Ionics **9&10**, 1347 (1983).

[2] A. Fontana, G. Mariotto, and M. P. Fontana, Phys. Rev. B **21**, 1102 (1980).

[3] R. Aronsson, L. Börjesson, and L. M. Torrell, Solid State Ionics **8**, 147 (1983).

[4] K. Funke, Adv. Solid State Phys. **20**, 1 (1980).

[5] P. Brüesch, W. Bührer, and H. J. M. Smeets, Phys. Rev. B **22**, 970 (1980).

[6] W. Andreoni and J. C. Phillips, Phys. Rev. B **23**, 645 (1981).

[7] (a) G. Szabó, J. Phys. C **19**, 3775 (1986); (b) G. Szabó and J. Kertész, *ibid.* **19**, L273 (1986).

[8] E. Cazzanelli, A. Fontana, G. Mariotto, V. Mazzacurati, G. Ruocco, and G. Signorelli, Phys. Rev. B **28**, 7269 (1983).

[9] W. Dieterich, P. Fulde, and I. Peschel, Adv. Phys. **29**, 527 (1980).

[10] (a) A. Rahman and P. Vashishta, Phys. Rev. Lett. **50**, 1073 (1983); see also *The Physics of Superionic Conductors and Electrode Materials,* edited by J. Perram (Plenum, New York, 1983), pp. 93–141; (b) M. Parrinello, A. Rahman, and P. Vashishta, Phys. Rev. Lett. **50**, 1073 (1983).

[11] J. L. Tallon, Phys. Rev. B **38**, 9069 (1988).

[12] G. L. Chiarotti, G. Jacucci, and A. Rahman, Phys. Rev. Lett. **57**, 2395 (1986).

[13] Y. Kaneko and A. Ueda, J. Phys. Soc. Jpn. **55**, 3294 (1986).

[14] A. Kvist and A. Josephson, Z. Naturforsch. **239**, 625 (1968).

[15] H. U. Beyeler and S. Strässler, Phys. Rev. B **20**, 1980 (1979).

[16] C. M. Perrott and N. H. Fletcher, J. Chem. Phys. **50**, 2770 (1969).

[17] G. Mariotto, A. Fontana, E. Cazzanelli, F. Rocca, M. P. Fontana, V. Mazzacurati, and G. Signorelli, Phys. Rev. B **23**, 4782 (1981).

[18] V. Mazzacurati, G. Ruocco, G. Signorelli, E. Cazzanelli, A. Fontana, and G. Mariotto, Phys. Rev. B **26**, 2216 (1982).

[19] M. P. Allen and D. Tildesley, *Computer Simulation of Liquids* (Oxford University, New York, 1987).

[20] *International Tables for X-Ray Crystallography* (Kynoch, Birmingham, U.K., 1973), Vol. 3; *ibid.* (Kynoch, Birmingham, U.K., 1974), Vol. 4.

[21] S. F. Lovesey, *Theory of Neutron Scattering* (Clarendon, Oxford, 1984).

[22] F. Willaime and C. Massobrio, Phys. Rev. Lett. **63**, 2244 (1989).

[23] U. Köhler and C. Herzig, Philos. Mag. A **58**, 769 (1988).

[24] M. Klein, in *Molecular Dynamics Simulations of Statistical Mechanical Systems,* edited by G. Ciccotti and W. G. Hoover (North-Holland, Amsterdam, 1986).

[25] B. Berne and R. Pecora, *Dynamic Light Scattering* (Wiley In-

terscience, New York, 1976).
[26]R. Loudon and W. Hayes, *Scattering of Light by Crystals* (Wiley, New York, 1978).
[27]P. A. Madden and R. W. Impey, Chem. Phys. Lett. **123**, 502 (1986).
[28]P. W. Fowler and P. A. Madden, Phys. Rev. B **31**, 5443 (1985).
[29]J. Board and P. A. Madden, J. Chem. Soc. Faraday Trans. II **83**, 1891 (1987).
[30]P. A. Madden, K. F. O'Sullivan, J. A. Board, and P. W. Fowler, J. Chem. Phys. **94**, 918 (1991).
[31]K. O'Sullivan, P. A. Madden, and G. L. Chiarotti (unpublished).